

Article

New Unequal Error Protection Strategy for Image Transmission Based on Bilayer-Lengthened PLDPC Code in Half-Duplex Relay System

Tian Gao ¹, Min Xiao ^{1,*}, Pingping Chen ^{2,*} and Diyan Gao ³

¹ School of OPTO-Electronic and Communication Engineering, Xiamen University of Technology, Xiamen 361005, China

² School of Physics and Information Engineering, Fuzhou University, Fuzhou 350108, China

³ Maynooth International School of Engineering, Fuzhou University, Fuzhou 350108, China

* Correspondence: xiaomin_ced@xmut.edu.cn (M.X.); ppchen.xm@gmail.com (P.C.)

Abstract: To reduce the waste of energy in communications, unequal error protection (UEP) is used to provide asymmetric protection for messages with different levels of importance. This paper proposes new efficient strategies of UEP based on bilayer protograph-based low-density parity check (PLDPC) codes in decoding-and-forward (DF) relay systems. In particular, we jointly utilize source coding and channel coding to design UEP strategies and then save transmission energy. According to the different levels of importance of discrete cosine transform (DCT) coefficients of image and variance statistical characteristics of image sub-blocks, bilayer-lengthened PLDPC codes are exploited to protect the transmitted image information with different importance levels at the half-duplex relay system. In the end, the simulation result shows that the proposed UEP schemes achieve excellent performance gains compared to conventional equal error protection (EEP) scheme. Additionally, the complexity analysis of the UEP strategies is given.

Keywords: bilayer PLDPC; unequal error protection; joint source-channel coding; image segment



Citation: Gao, T.; Xiao, M.; Chen, P.; Gao, D. New Unequal Error Protection Strategy for Image Transmission Based on Bilayer-Lengthened PLDPC Code in Half-Duplex Relay System. *Symmetry* **2022**, *14*, 1662. <https://doi.org/10.3390/sym14081662>

Academic Editor: Dumitru Baleanu

Received: 6 July 2022

Accepted: 3 August 2022

Published: 11 August 2022

Publisher's Note: MDPI stays neutral with regard to jurisdictional claims in published maps and institutional affiliations.



Copyright: © 2022 by the authors. Licensee MDPI, Basel, Switzerland. This article is an open access article distributed under the terms and conditions of the Creative Commons Attribution (CC BY) license (<https://creativecommons.org/licenses/by/4.0/>).

1. Introduction

In recent years, many research activities both on the coding and decoding of cooperative communication schemes have attracted a lot of attention [1–3]. Relay cooperative communication has won increasingly broad applications for its high ability of anti-fading in wireless multi-path channels, improving the reliability of information transmission [4,5]. Since the wireless co-operation communications utilize additional relay nodes, the cost of energy increases accordingly. Thus, improving the energy efficiency is one of the important issues in this co-operation system. Reference [6] considered the joint utility-based uplink power and rate allocation to raise the efficiency of energy in communication, and reference [7,8] studied the performance of resource allocation in non-orthogonal multiple access- (NOMA) based networks to solve the efficiency maximization problem of the downlink NOMA-based, massive multiple-input-multiple-output (MIMO) system.

As information is becoming more diversified and complicated, distinguishing information of different importance levels and providing asymmetric protection is essential to cater to the requirements of high performance and low transmission power nowadays. Reference [9] proposed a concept of unequal error protection (UEP) for channel coding that reduces energy consumption by providing different levels of protection for information with different levels of importance. Reference [10] presented rate allocation optimization algorithms based on rate-compatible codes for embedded image bit streams transmitted over noisy channels under UEP. Reference [11] proposed a UEP scheme by tracing the mapping between the important information data and the elite bits of an irregular LDPC code.

Reference [12] proposed a good tradeoff UEP-scheme between reliability and spectrum efficiency by using sixteen quadrature amplitude modulation (QAM) mapping. Reference [13] realized UEP by classifying the bit-channel type based on the delayed bit-interleaved coded modulation (DBICM). Reference [14] took advantage of the adaptive segmentation and weight-increase parity check (WIPC) LDPC code to achieve UEP for image sources. A UEP scheme based on the Luby transform (LT) codes was proposed in [15] for image transmission over multiple-input-multiple-output (MIMO) channels. Reference [16] presented a novel autoencoder-based approach for designing codes that provide UEP capabilities, and reference [17] proposed a type-aware coding approach to achieve UEPs for multiple classes of messages.

In this paper, we design two UEP strategies based on bilayer protograph-based LDPC (PLDPC) codes in a half-duplex relay system. PLDPC code is a subclass of LDPC codes [18,19], which benefit from simple structures and desirable performance in wireless applications [20–25]. Bilayer PLDPC code was put forward in decoding-and-forward (DF) relay systems. It is an especially useful class of structured LDPC codes and more general multi-layer codes and allows decoding of the same codeword with two (or more) different decoders [26–28]. We find that most existing UEP strategies focused on the implementation of channel coding without considering the characteristics of the source, and the optimization methods of these UEP-based codes are relatively complex. Thus, to address this issue, we exploit lengthened bilayer-lengthened PLDPC codes in UEP to transmit the information of different source characteristics. Bilayer PLDPC code can perform remarkably in this case due to its advantages, such as low encoding complexity, modular structure for easy design, and rate compatibility. Moreover, bilayer PLDPC code under the UEP scheme in relay systems can match a set of channel conditions without extensive re-optimization. Based on this, we propose two new UEP strategies with excellent performance. The main contributions of this work are summarized as follows:

- (1) This paper proposes the concept that the integer and decimal parts of DCT coefficients have different levels of importance instead of considering high-frequency and low-frequency components of DCT coefficients with different levels of importance traditionally. Based on this, a joint source-channel coding UEP scheme (UEP-1) is designed based on bilayer-lengthened PLDPC code in half-duplex relay systems.
- (2) This paper further proposes an elaborate UEP scheme (UEP-2) with excellent performance. We can realize UEP for image sub-blocks information with different levels of importance by variable rates and only need to store one bilayer protograph base matrix without extensive re-optimization. It reduces the required cache space for practical applications greatly. In the UEP-2 scheme, image sub-blocks are assigned to the corresponding class according to the classification map generated by K-means clustering.

At last, the simulation results show that the proposed UEP-1 scheme has 0.8 dB and 0.3 dB gains, and the proposed UEP-2 scheme has 1.6 dB and 1.1 dB gains compared to EEP and the traditional UEP scheme in low and high SNR regions, respectively. Compared to the traditional UEP scheme, both UEP-1 and UEP-2 schemes can achieve better performance. Moreover, we compare the FSIM between the recovered image and the original image under different SNRs, which shows that the performance of proposed UEP scheme is superior to that of EEP scheme. The complexity analysis of UEP strategies is given by discussing the usage of modules and computing the average number of decoding iterations.

2. Preliminaries and Notations

The table of notations in this section is shown in Table 1.

Table 1. Notations in Section 2.

<u>Section 2.1</u>	
B	Protograph base matrix
H	Protograph LDPC matrix
v	Variable node
c	Check node
Z	Lifting factor from protograph base matrix to protograph LDPC matrix
N_p	The number of variable nodes in the protograph base matrix
N	The number of variable nodes in the protograph LDPC matrix
M_p	The number of check nodes in the protograph base matrix
M	The number of check nodes in the protograph LDPC matrix
K	The number of information bits in the protograph LDPC code
<u>Section 2.2</u>	
B_{sd}	Bilayer-lengthened protograph base matrix with a lower rate
B_e	Extension base matrix
B_{sr}	Bilayer-lengthened protograph base matrix with high rate extended by B_{sd}
<u>Section 2.3</u>	
X_1	The broadcasted signal from the source during time slot one
X_2	The broadcasted signal from the source during time slot two
Y_1	Received signal in the destination during time slot one
Y_2	Received signal in the destination during time slot two
V_1	Received signal in the relay during time slot one
L_2	The transmitted signal from the relay to the destination during time slot two
Z_{sr}	Additive Gaussian noise received by the relay
Z_{d1}	Additive Gaussian noise received by destination during time slot one
Z_{d2}	Additive Gaussian noise received by destination during time slot two
P_{s1}	The power constraint of the source during time slot one
P_{s2}	The power constraint of the source during time slot two
P_{R_2}	The power constraint of the relay during time slot two
SNR_{ij}	Signal-to-noise ratio between node i and node j

2.1. Protograph LDPC Code

Protograph LDPC codes define a subclass of multi-edge type LDPC (MET-LDPC) codes, which allow extending a base matrix or graph prototype (base graph) to a complete matrix or graph [28]. A well-designed protograph LDPC code can achieve better performance and is suitable for an efficient encoding/decoding implementation [29,30]. A protograph $B = (\mathcal{V}, \mathcal{C}, \mathcal{E})$ can be represented by a tanner graph with a relatively small number of nodes, which consists of three sets, \mathcal{V} , \mathcal{C} and \mathcal{E} , corresponding to N_p variable nodes (VNs), M_p check nodes (CNs), and the connecting edges, respectively. Each edge $e_{i,j} \in \mathcal{E}$ connects a VN $v_j \in \mathcal{V}$ to a CN $c_i \in \mathcal{C}$. A graphical example of generating the derived graph is shown in Figure 1. An (N, K) protograph code (an equivalent LDPC code) is derived by using a process known as *lifting*, where N and $N - K$ equals the number of VNs and CNS in the derived tanner graph corresponding to the base protograph graph, respectively. The *lifting* process utilizes the copy-and-permutation operation. The number of copy times is decided by the lifting factor $Z = N/N_p = M/M_p$, where $M = N - K$.

2.2. Bilayer-Lengthened PLDPC Code

Graph Structure: Geometrically, the variable nodes are divided into two layers: *layer-1* and *layer-2*, and the check nodes are all in one set in a bilayer-lengthened protograph [27]. Figure 2 shows that the edges of the base graph are connected in the first layer of variable nodes with the set of check nodes forming a base graph with a lower rate. The entire edges and nodes constitute a base graph with a high rate. The rate of bilayer-lengthened PLDPC code can be increased by adding the number of variable nodes in *layer-2*.

The entire protograph base matrix has the form

$$B_{sr} = [B_{sd}|B_e] \quad (1)$$

where B_{sd} is the protograph base matrix with a lower rate corresponding to *layer-1*, and B_e is the extension base matrix corresponding to *layer-2* in the tanner graph.

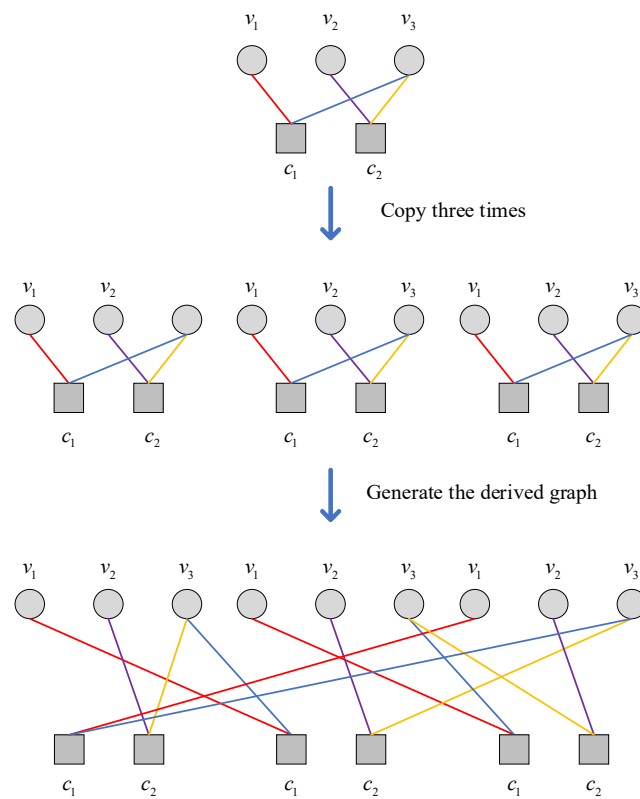


Figure 1. A graphical example of generating the derived graph.

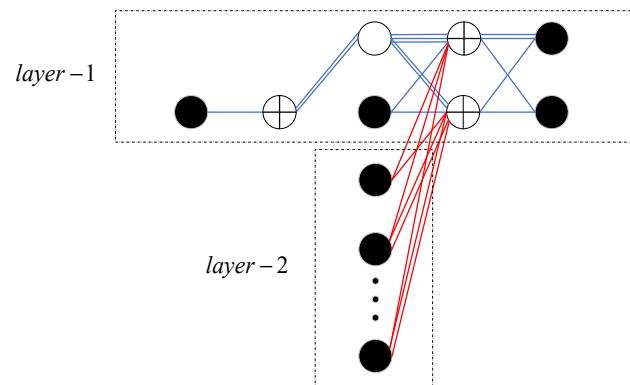


Figure 2. A Tanner graph of bilayer-lengthened photograph. Black circles and circles with plus represent VNs and CNs, respectively, and the blank circle denotes the VNs which have been punctured.

2.3. Half-Duplex Relay System

According to the classic work of Cover and El Gamal [31], DF protocol describes that the relay completely decodes the transmitted message from the source and partially forwards the decoded message to the destination. In the destination, the receiver recovers the message by processing the signals transmitted by the source and relay. Half-duplex relay system is widely studied system in practice. This paper exploits the novel UEP scheme for the half-duplex relay system, where the relay can communicate with only one node in a time slot. According to [31] and Figure 3, the received signal in a half-duplex relay channel can be given by

$$V_1 = h_2 X_1 + Z_{sr} \tag{2}$$

$$Y_1 = h_1 X_1 + Z_{d1} \tag{3}$$

$$Y_2 = h_1 X_2 + h_3 L_2 + Z_{d2} \tag{4}$$

where X_1 , Y_1 , and V_1 denote the transmitted signal from a source (**S**), the received signal in the destination (**D**), and the relay (**R**) during time slot one (a fraction t_1 of the transmission interval), respectively. X_2 , L_2 , and Y_2 denote the transmitted signals from source, relay, and the received signals in the destination during time slot two (a fraction $t_2 = 1 - t_1$), respectively. h_1 , h_2 , and h_3 are **S**-to-**D**, **S**-to-**R**, and **R**-to-**D** channel coefficients, respectively. $Z_{sr} \sim N(0, \sigma_{sr})$, $Z_{d1} \sim N(0, \sigma_{sd})$, and $Z_{d2} \sim N(0, \sigma_{sr} + \sigma_{rd})$ denote additive Gaussian noises at the relay and at destination for time slot one and time slot two, respectively. In time slots one and two, the communication channel can be seen as a broadcast channel and a multi-access channel, respectively. The source has power constraint $P_{S1} = E(X_1^2)$ in time slot one and power constraint P_{S2} in time slot two. P_{R2} represents relay power constraint in time slot two. Thus, signal-to-noise ratios (SNR) SNR_{SR} , SNR_{SD} , and SNR_{RD} can be defined at the relay and destination at time slot one and at the destination at time slot two, respectively.

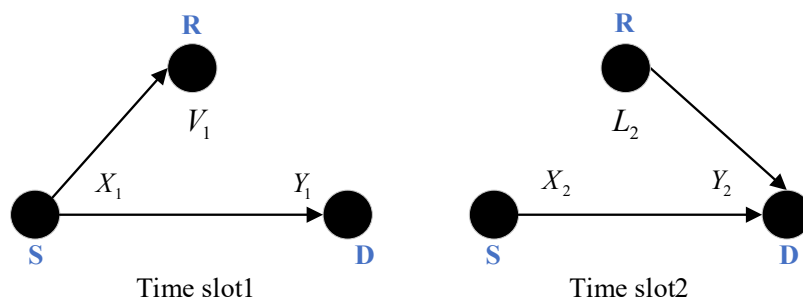


Figure 3. Half-duplex relay channel.

3. New UEP Strategy

3.1. UEP System Model

For practical purposes, we consider gray images as research objects for the UEP strategy in this paper. A new UEP scheme (UEP-1) system model in a half-duplex relay system is shown in Figure 4. After block discrete cosine transform (DCT) [32,33] processing of the input image, we found that each DCT coefficient Q can be divided into two parts—the integer part Q_i and the decimal part Q_d , where Q_d is approximated by retaining the binary number of k bits. The recovery performance of the image is dependent on the size of k . The degradation coefficients Q' can be represented as

$$Q' = \begin{cases} Q_i + Q_d, & \text{if } Q \geq 0 \\ Q_i - Q_d, & \text{if } Q < 0 \end{cases} \tag{5}$$

where if $Q \geq 0$, $Q_i = \lfloor Q \rfloor$ and $Q_d = Q - Q_i$; else $Q_i = \lceil Q \rceil$ and $Q_d = Q_i - Q$. This step not only conserves transmission quality significantly, but also facilitates the combination of image transmission and UEP strategy. Q_i and Q_d have different attribution to Q' . In binary, Q' has a deviation of 2^i when an error happens in the i -th bit of Q_i . In contrast, only $(\frac{1}{2})^i$ deviation in Q' when an error happens in the i -th bit of Q_d . Thus, the proposed UEP strategy provides two transmission paths for Q_i and Q_d . For Q_d with less attribution to Q' , a traditional point-to-point channel (S-D link) coding and decoding mode is adopted. For Q_i with much attribution to Q' , the relay transmits additional mutual information to help

the destination decode the source message. In the destination, estimated information \tilde{Q}_i and \tilde{Q}_d are decoded, and the estimated DCT coefficient \tilde{Q} can be estimated by

$$\tilde{Q} = \begin{cases} \tilde{Q}_i + \tilde{Q}_d, & \text{if } \tilde{Q}_i \geq 0 \\ \tilde{Q}_i - \tilde{Q}_d, & \text{if } \tilde{Q}_i < 0 \end{cases} \quad (6)$$

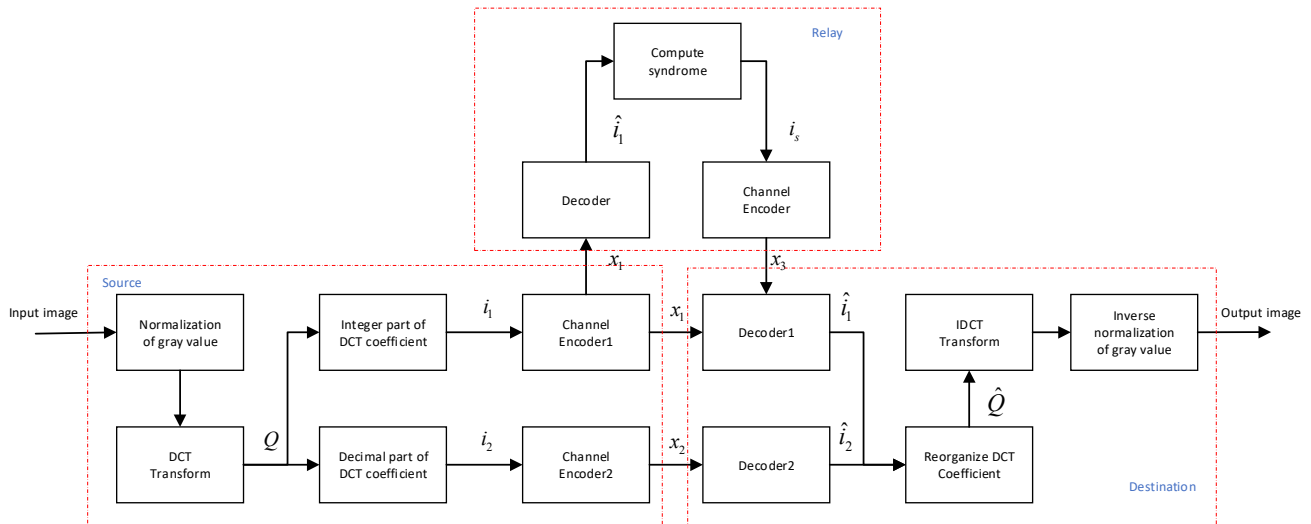


Figure 4. An UEP system model based on half-duplex relay system.

At last, the image can be restored by two steps, such as inverse discrete cosine transform (IDCT) and inverse normalization.

Encoding/Decoding of UEP System

The encoding of the UEP strategy only needs to store the bilayer protograph base matrix B_{sr} , extending by a lower-rate bilayer protograph base matrix B_{sd} , $B_{sr} = [B_{sd}|B_e]$. The signal i_1 of integer parts and the signal i_2 of decimal parts are encoded by H_{sr} (lift from B_{sr}) to generate the codewords x_1 and x_2 by encoder1 and encoder2, respectively. Encoder2 sends the codeword $x_2 = G_{sr}^T i_2$ to the destination, and encoder1 broadcasts the codeword $x_1 = G_{sr}^T i_1$ to relay and destination. G_{sr} is the generating matrix of parity check matrix H_{sr} . The relay encodes the syndrome i_s and transmits codeword x_3 to the destination by

$$x_3 = G_{sd}^T i_s \quad (7)$$

where $i_s = \tilde{i}_1^T H_{sd}^T$, and \tilde{i}_1 is the estimated information corresponding to variable nodes in *layer-2*, which is extracted from the estimated information \tilde{i}_1 . Estimated information \tilde{i}_1 have been decoded from x_1 at the relay. H_{sd} is lifted from the base matrix B_{sd} .

Figure 5a,b show the iterative decoding factor graphs in decoder1 and decoder2. In Figure 5a, the variable nodes in *layer-2* are checked by the parity check matrix H_{sr} . The additional Log-Likelihood Ratio (LLR) of variable nodes in *layer-2* provide help for decoding the variable nodes in *layer-1*. We can see that the message from the j -th check node to the i -th variable node is

$$L(r_{ji}) = 2 \tanh^{-1} \left(\prod_{i' \in R(j)/i} \tanh(L(q_{i'j})/2) \right) \quad (8)$$

where $q_{i'j}$ is the message from i' -th variable node to j -th check node, and i' belongs to set $R(j)/i$. The elements in $R(j)/i$ can be divided into two parts corresponding to *layer-1* and *layer-2*. Compared to decoder2 in Figure 5b, decoder1 has a much more reliable message

from the variables nodes that are connected to the syndrome in *layer-2*. It suggests a more reliable LLR $L(q_i)$ for the i -th variable node, computed by

$$L(q_i) = L(P_i) + \sum_{j \in C(i)} L(r_{ji}) \tag{9}$$

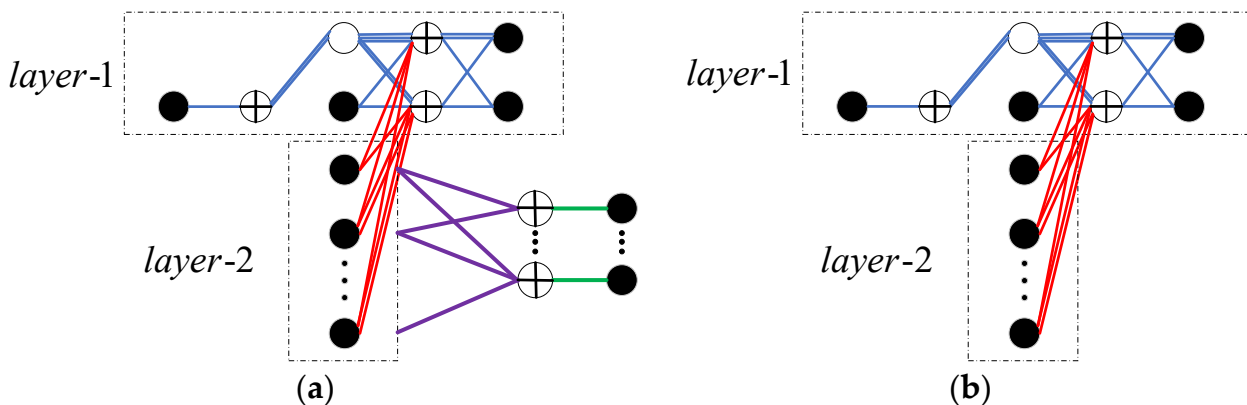


Figure 5. (a) Factor graph for decoder1. (b) Factor graph for decoder2.

3.2. Image Segmentation UEP Strategy

The image segmentation UEP strategy is illustrated in Figure 6. In this diagram, the classification map is generated by K-means clustering. In the source, the classification map is used to order sub-blocks of an input image and choose bilayer matrix with different rates for sub-blocks in different classes. Integer parts of DCT coefficients are encoded by bilayer PLDPC code with a fixed rate. Decimal parts of DCT coefficients are encoded by bilayer PLDPC code with a certain rate that is chosen from the classification map. Transmission message $x_s = [x_1, x_2]$ is broadcasted to the relay and the destination in time slot 1, respectively. The relay sends the message $x_3 = G_{sd}^T i_s$ to destination after decoding the message x_s and computing syndrome i_s . DCT coefficients can be recovered after decoding \hat{x}_s in destination. A recovery image is obtained by reordering the sub-blocks with a classification map known at the receiver. We describe the main two steps of the UEP scheme (UEP-2) in this section, such as the image segmentation and the encoding procedure.

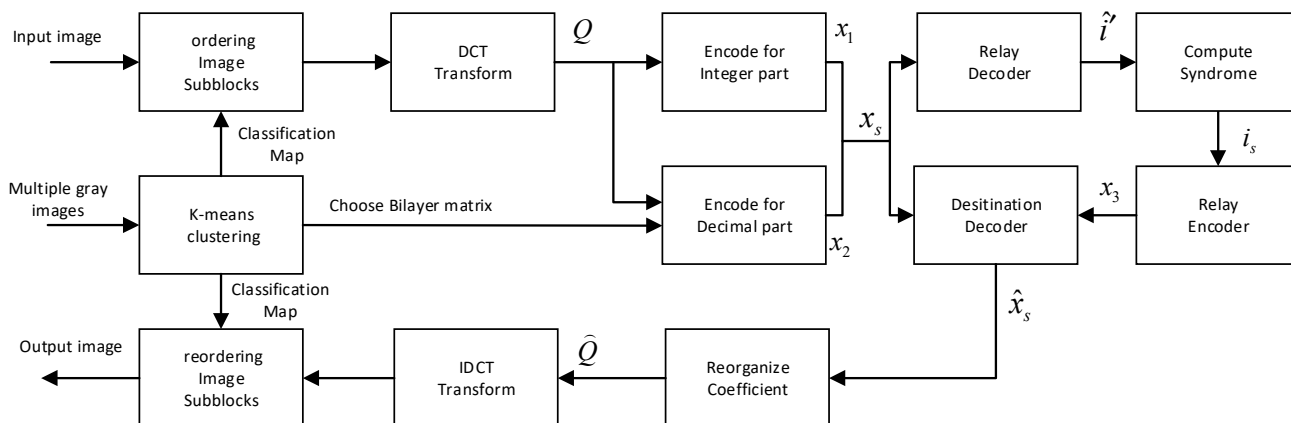


Figure 6. The frame diagram of the image segmentation UEP scheme.

3.2.1. Image Segmentation

To segment the original image of size (M, N) and distinguish sub-blocks of different levels of importance from all sub-blocks, we can discover the intensity of the pixel of sub-blocks change by defining the variance σ of the sub-blocks,

$$\sigma = \frac{\sum_{i=1}^m \sum_{j=1}^n (x_{i,j} - \bar{x})^2}{m \times n} \quad (10)$$

$$\bar{x} = \frac{\sum_{i=1}^m \sum_{j=1}^n x_{i,j}}{m \times n} \quad (11)$$

where $x_{i,j}$ represents the value of the pixel of the sub-blocks, and m and n are the size of the sub-blocks. An original image can be segmented into $z = M/m = N/n$ sub-blocks, and an array of variances $\sigma = [\sigma_1, \sigma_2, \dots, \sigma_z]$ can be computed corresponding to z sub-blocks. Then, the variance matrix of sub-blocks of k images can be represented by

$$(\mathbf{s}_1 \quad \dots \quad \mathbf{s}_z) = \begin{pmatrix} \sigma_{1,1} & \dots & \sigma_{1,z} \\ & \ddots & \\ \sigma_{k,1} & \dots & \sigma_{k,z} \end{pmatrix} \quad (12)$$

where $\sigma_{i,j}$ denotes the variance of the j -th sub-block in the i -th image, and column vector \mathbf{s}_j represents the variances of the j -th sub-block of all the images. The classes are developed by K-means clustering [34] to classify sub-blocks from multiple images (except for the images waiting for transmission).

3.2.2. Encoding of Image Segmentation UEP Strategy

Assuming that sub-blocks of the input image are divided into four groups by classification map, for sorted sub-blocks of the input image, we match the integer parts signal i_1 of DCT coefficients with a fixed lower-rate bilayer PLDPC code $H_{sr,1}$ and decimal parts signal i_2 of DCT coefficients with diverse rates bilayer-lengthened code $H_{sr,i}$, $i \in [1, 2, 3, 4]$, by

$$x_1 = G_{sr,1}^T i_1 \quad (13)$$

$$x_{2,i} = G_{sr,i}^T i_{2,i} \quad (14)$$

where $i_2 = [i_{2,1}, i_{2,2}, i_{2,3}, i_{2,4}]$ are the decimal parts of DCT coefficients after ordering all of the image sub-blocks, and $i_{2,i}$ corresponds to the i -th group that decimal parts of sub-blocks belong to. The source broadcasts codeword $x_s = [x_1, x_2]$ to the relay and destination, where $x_2 = [x_{2,1}, x_{2,2}, x_{2,3}, x_{2,4}]$. $G_{sr,i}$ denotes the generator matrix of the parity check matrix $H_{sr,i}$ lifting from $B_{sr,i}$. $B_{sr,i}$ is a sub-protograph base matrix with a higher rate extended by

$$B_{sr,1} = [B_{sd} | B_e] \quad (15)$$

$$B_{sr,2} = [B_{sr,1} | B_{e,1}] \quad (16)$$

$$B_{sr,i} = [B_{sr,i-1} | B_{e,i-1}] \quad (17)$$

As can be seen in Equations (15)–(17), diverse rates can be achieved for the decimal parts of DCT coefficients of sub-blocks with different levels of importance by the matrix expansion method, and only one base matrix $B_{sr,i}$ needs to be stored. $B_{sr,i-1}$ and $B_{e,i-1}$ corresponding to *layer-1* and *layer-2* are combined to create a capacity-approaching code for image transmission.

Relay decodes the codeword x_s and extracts the second layer information \hat{i}_1 and \hat{i}_2 from x_1 and x_2 and then computes syndrome $i_s = [i_{s1} | i_{s2}]$, $i_{s1} = \hat{i}_1 H_{sd}^T$ and $i_{s2} = \hat{i}_2 H_{sd}^T$, respectively. As shown in Figure 6, codeword $x_3 = G_{sd}^T i_s$ is decoded at the destination, and

the syndrome i_s is recovered during the second time slot. With the recovered syndrome, we have bilayer PLDPC codes $H_{sr,1}$ and $H_{sr,i}$, as shown in Figure 7. The check relationship between *layer-2* variables nodes and syndrome nodes helps the destination with forming lower rate codes to decode the codeword x_s from the source.

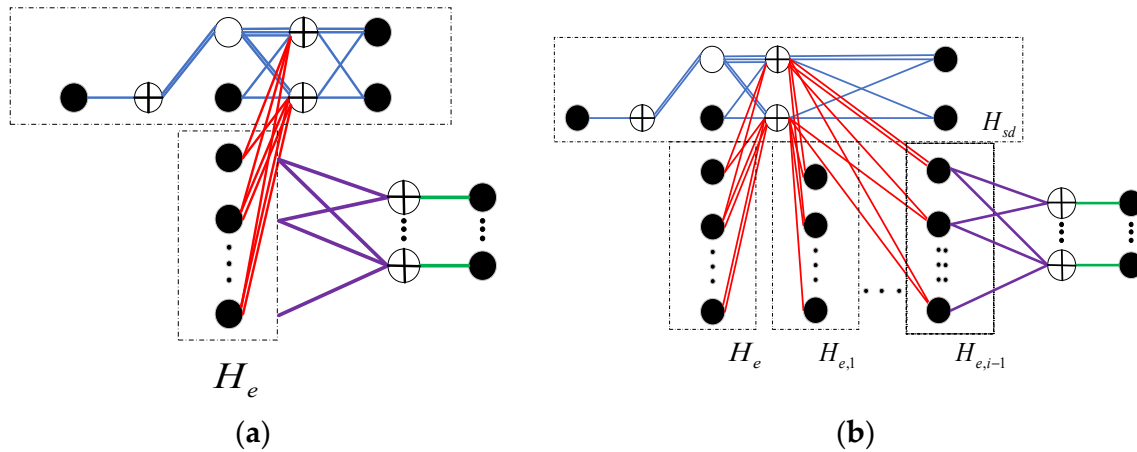


Figure 7. The tanner graph of bilayer PLDPC codes with the syndrome. (a) Bilayer PLDPC codes $H_{sr,1}$ with the syndrome; (b) Bilayer PLDPC codes $H_{sr,i}$ with the syndrome.

4. Results

4.1. Simulation Result

This part demonstrates the simulation performance of the proposed UEP schemes. The software and hardware platforms of simulation are C++, Matlab, Intel i7, and Nvidia 3060, respectively. The preset parameters are shown in Table 2; we compared three strategies, and the length of codes was 1296 in simulation. The first strategy (EEP) protected the integer and decimal parts of DCT coefficients of the image by the classical AR3A code with a 3/4 rate equally in the point-to-point channel (S-D link). The second strategy (UEP-1) provided UEP for the integer and decimal parts of DCT coefficients of the image. The integer and decimal parts were encoded by bilayer-PLDPC code H_{sr} with a 3/4 rate. The integer parts were transmitted in the relay channel while decimal parts were transmitted in the point-to-point channel (S-D link). The third strategy (UEP-2) utilized the image segmentation scheme and applied diverse rates (2/3, 3/4, 4/5, 5/6) of bilayer PLDPC codes for the decimal parts of DCT coefficients in four groups (classified by K-means clustering 40 images). The integer parts were encoded with a 2/3 rate bilayer PLDPC coded and were transmitted together with decimal parts in the half-duplex relay channel. The protograph base matrix $H_{1/2}$ and the corresponding extended sub-protograph base matrices $H_{2/3}$, $H_{3/4}$, $H_{4/5}$, and $H_{5/6}$ were optimized by protograph extrinsic information transfer (PEXIT) algorithm [28] as

$$H_{1/2} = \begin{pmatrix} 1 & 2 & 0 & 0 & 0 & 1 & 0 \\ 0 & 3 & 1 & 1 & 1 & 1 & 0 \\ 0 & 1 & 2 & 2 & 2 & 1 & 1 \\ 0 & 2 & 0 & 0 & 0 & 0 & 2 \end{pmatrix} \quad (18)$$

$$H_{2/3} = \left(H_{1/2} \left| \begin{array}{ccc} 0 & 1 & 1 \\ 1 & 1 & 1 \\ 2 & 1 & 2 \\ 0 & 1 & 0 \end{array} \right. \right), \quad H_{3/4} = \left(H_{2/3} \left| \begin{array}{ccc} 0 & 0 & 2 \\ 2 & 2 & 0 \\ 1 & 1 & 2 \\ 0 & 0 & 1 \end{array} \right. \right) \quad (19)$$

$$H_{4/5} = \left(H_{3/4} \left| \begin{array}{ccc} 0 & 1 & 2 \\ 1 & 2 & 2 \\ 2 & 1 & 1 \\ 0 & 0 & 0 \end{array} \right. \right), \quad H_{5/6} = \left(H_{4/5} \left| \begin{array}{ccc} 0 & 0 & 2 \\ 2 & 2 & 0 \\ 1 & 1 & 2 \\ 0 & 0 & 2 \end{array} \right. \right)$$

where $H_{2/3}$, $H_{3/4}$, $H_{4/5}$, and $H_{5/6}$ were lifted 216, 144, 108, and 87 times to achieve the 1296 code length corresponding to bilayer-PLDPC full matrices $H_{sr,1}$, $H_{sr,2}$, $H_{sr,3}$, and $H_{sr,4}$ respectively. The end-to-end relay channel error can be presented as a function of the three SNRs (SNR_{sd} , SNR_{sr} , and SNR_{rd}) of its constituent channels, represented by

$$SNR_{SR} = SNR_{SD} + a, SNR_{RD} = SNR_{SD} + b \tag{20}$$

where a and b are variable parameters [28].

Table 2. Simulation parameter setting.

Parameters	EEP	UEP-1	UEP-2
Code length	1296	1296	1296
Code rate	3/4	3/4	2/3, 3/4, 4/5, 5/6
a (dB)	no relay	1.4	1.4
b (dB)	no relay	1.6	1.6

Figure 8 shows the end-to-end performance comparison of different bilayer PLDPC code and the conventional AR3A code in half-duplex relay system. It is observed that the bilayer PLDPC codes had performance gains of 0.3 dB and 0.2 dB over the AR3A code at rates of 2/3 and 3/4, respectively.

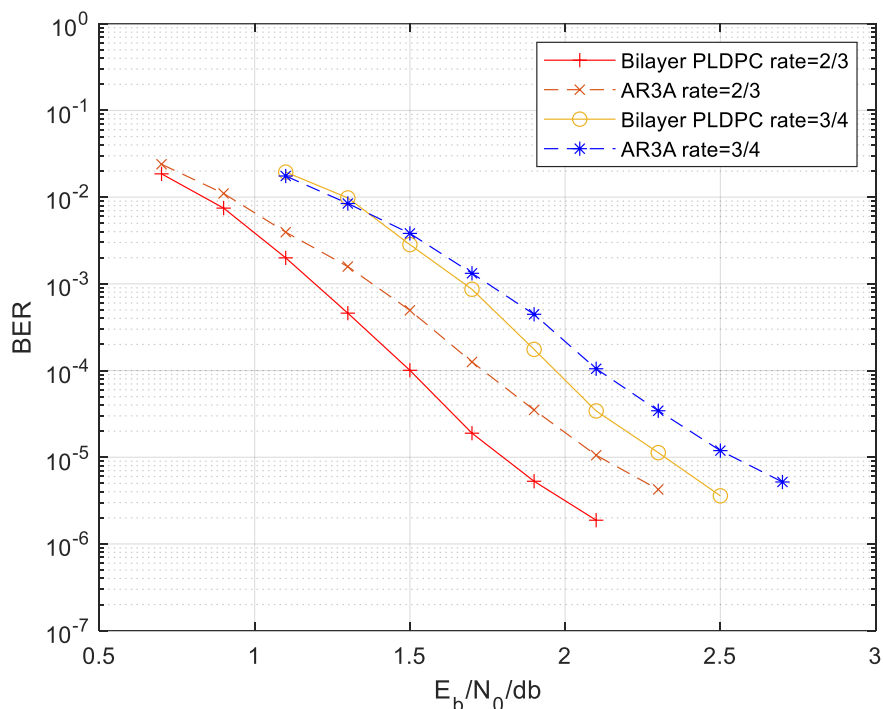


Figure 8. The end-to-end performance comparison of bilayer-lengthened PLDPC code and AR3A code in in half-duplex relay system.

Figure 9 shows the performance of recovery image of the three strategies with $SNR_{SD} = 1.3, 1.9, 2.1$ dB, $a = 1.4$, and $b = 1.6$. We can see that the recovery image qualities of the UEP-1 and UEP-2 strategies were significantly better than that of the EEP strategy under different SNRs. The UEP-1 and UEP-2 strategies achieved 19 dB and 31 dB peak signal-to-noise ratio (PSNR) gain over the EEP scheme for image ‘Pepper’ at $SNR_{SD} = 2.5$ dB, respectively.



Figure 9. The comparison of recovery images in 3 strategies.

Figure 10 demonstrates the comparison of the PSNR of recovered images in four schemes under different SNRs. The AR3A code with a threshold at 3.1 dB was utilized for both integer and decimal parts of DCT coefficients in the EEP scheme. The UEP-0 scheme is the mainstream UEP method in joint source-channel coding system, which provides UEP for the high and low frequency of DCT coefficients [14]. The UEP-1 and UEP-2 schemes were designed in Sections 3.1 and 3.2, respectively. As can be seen in Figure 10, the ‘Lena’ image can be recovered at 3.1 dB and 3 dB by EEP and UEP-0 schemes, respectively. Compared to EEP and UEP-0 schemes, the UEP-1 scheme can achieve 0.3 dB and 0.2 dB gains, and the gains are higher in the low SNR region, reaching 0.8 dB and 0.6 dB, respectively. The UEP-2 scheme provides a delicate UEP strategy for decimal parts of DCT coefficients by image segmentation. As shown in Figure 10, UEP-2 had 0.8 dB and 0.7 dB gains in high SNR regions and 1.3 dB and 1.1 dB gains in the low SNR region, in contrast to the EEP and UEP-0 schemes, respectively.

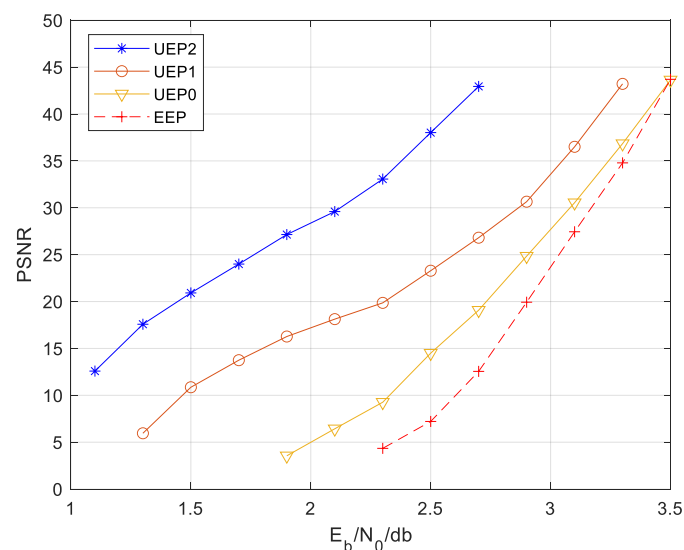


Figure 10. The PSNR comparison of ‘Lena’s recovery image in 4 protection strategies.

Furthermore, Figure 11 shows the comparison of the feature similarity index measure (FSIM) between the recovery image and original image in three schemes under different SNRs. We can see the FSIM achieved 0.99 at 1.5 dB in the UEP-2 scheme, which is superior to those of UEP-1 and EEP of 1 dB and 1.3 dB, respectively. Moreover, it is interesting to note that the FSIM goes up to the top very quickly in the EEP scheme, compared to the proposed UEP schemes. This is due to that the decimal part of the DCT coefficients focuses on describing the details of the image, and this part of information can be recovered at high the SNR region in the proposed UEP schemes.

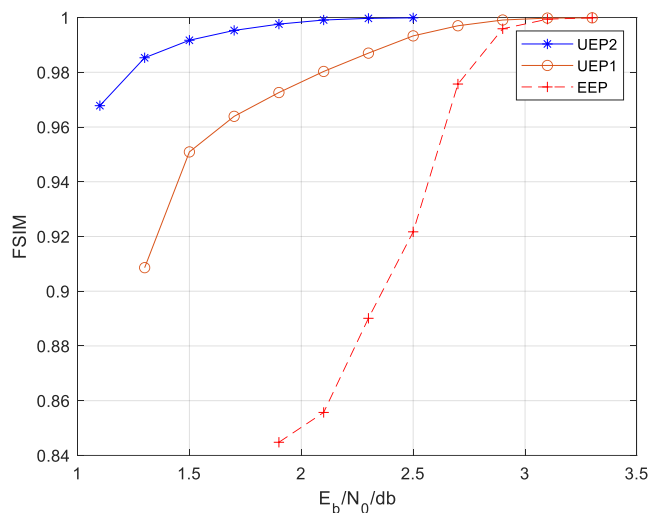


Figure 11. The FSIM comparison of ‘Lena’s recovery image in 3 protection strategies.

4.2. Complexity Analysis

The complexity of proposed joint source-channel coding frameworks is discussed in this section. As shown in Table 3, we tracked the usage of different modules in three strategies. In UEP-2, the module of reordering image sub-block is needed as compared to EEP and UEP-1. Since K-means clustering classifies the image sub-blocks into p groups, additional p times reordering operations are required. Moreover, both UEP-1 and UEP-2 strategies require the module to distinguish image source and additional l rounding operations and $2l$ addition operations for telling the integer and decimal source apart, where l is the number of the transmitted DCT coefficients. Furthermore, we considered the complexity of channel decoding in the three strategies. As shown in Table 3, both UEP-1 and UEP-2 strategies required the relay decoding and the joint decoding modules at the destination.

Table 3. The usage of modules in three transmission strategies.

Strategy	Modules in Three Strategies			
	Reordering Image Sub-Block	Distinguish Image Source	Relay Decoding	Destination Joint Decoding
EEP	no	no	no	no
UEP-1	no	yes	yes	yes
UEP-2	yes	yes	yes	yes

Moreover, we show the convergence of the BP decodings by calculating the average number of decoding iterations, as given in Figure 12. It can be observed that UEP-1 had about two more iterations in comparison to EEP, even if extra decoders were added in the relay and the destination. While UEP-2 had significantly higher iterations than EEP, the

main reason is that the relay and the destination need to use more decoding resources to decode the encoding message of the decimal part.

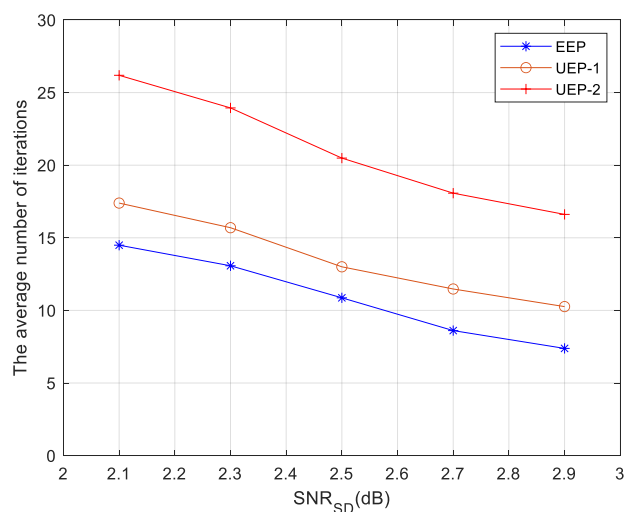


Figure 12. The average number of decoding iterations comparison in three strategies.

5. Discussion and Conclusions

A novel joint source-channel coding scheme is introduced into the half-duplex relay system to design a UEP strategy for image transmission in this paper. According to the different levels of importance of image DCT coefficients and variance statistical characteristics of image sub-blocks, two kinds of image non-symmetric protection strategies were proposed and realized based on a family of bilayer-lengthened PLDPC codes. The first UEP scheme is designed for different parts of DCT coefficients with different transmission strategies. The second UEP scheme provides non-symmetric protection for image sub-blocks with different levels of importance that are segmented from the original image. The simulation results show that the proposed UEP schemes both have excellent performance compared to the conventional EEP and UEP scheme in the half-duplex relay systems. In the end, some prospects are put forward. Note that it is hard to achieve the optimal image segmentation technique for UEP strategy. More excellent UEP strategy needs to be studied, such as the joint design of the image feature extraction technique [35–38] and channel coding technique. It is expected that the unequal error protection for the integers and decimals can be applied to various occasions, in addition to image transmission, when applying source-channel coding methods. Additionally, note that the optimization design for source structures and the bilayer PLDPC codes in UEP strategy deserves our further study.

Author Contributions: Conceptualization, T.G. and M.X.; methodology, T.G.; software, T.G.; validation, M.X., P.C. and D.G.; formal analysis, D.G.; investigation, T.G.; resources, M.X.; data curation, T.G.; writing—original draft preparation, T.G.; writing—review and editing, T.G. and P.C.; visualization, D.G. and P.C.; supervision, M.X.; project administration, M.X.; funding acquisition, M.X. All authors have read and agreed to the published version of the manuscript.

Funding: This research was supported the by Natural Science Foundation of Fujian Province, China under Grant no 2018J01569.

Institutional Review Board Statement: Not applicable.

Informed Consent Statement: Not applicable.

Data Availability Statement: Not applicable.

Conflicts of Interest: The authors declare no conflict of interest.

References

1. Li, Q.; Yu, M.; Pandharipande, A.; Ge, X. Outage Analysis of Co-Operative Two-Path Relay Channels. *IEEE Trans. Wirel. Commun.* **2016**, *15*, 3157–3169. [[CrossRef](#)]
2. Chen, P.; Xie, Z.; Fang, Y.; Chen, Z.; Mumtaz, S.; Rodrigues, J.J.P.C. Physical-Layer Network Coding: An Efficient Technique for Wireless Communications. *IEEE Netw.* **2020**, *34*, 270–276. [[CrossRef](#)]
3. Chen, P.; Liew, S.C.; Shi, L. Bandwidth-Efficient Coded Modulation Schemes for Physical-Layer Network Coding with High-Order Modulations. *IEEE Trans. Commun.* **2017**, *65*, 147–160. [[CrossRef](#)]
4. Hunter, T.E.; Nosratinia, A. Diversity through Coded Cooperation. *IEEE Trans. Wirel. Commun.* **2006**, *5*, 283–289. [[CrossRef](#)]
5. Rossetto, F.; Zorzi, M. Mixing Network Coding and Cooperation for Reliable Wireless Communications. *IEEE Wirel. Commun.* **2011**, *18*, 15–21. [[CrossRef](#)]
6. Tsiropoulou, E.E.; Vamvakas, P.; Papavassiliou, S. Joint Utility-Based Uplink Power and Rate Allocation in Wireless Networks: A non-cooperative game theoretic framework. *Phys. Commun.* **2013**, *9*, 299–307. [[CrossRef](#)]
7. El-ghorab, M.A.; El-meligy, M.R.; Ibrahim, M.M.; Newagy, F. Energy-Efficient User Pairing for Downlink NOMA in Massive MIMO Networks. *Appl. Sci.* **2022**, *12*, 5421. [[CrossRef](#)]
8. Ali, Z.J.; Noordin, N.K.; Sali, A.; Hashim, F.; Balfaqih, M. Novel Resource Allocation Techniques for Downlink Non-Orthogonal Multiple Access Systems. *Appl. Sci.* **2020**, *10*, 5892. [[CrossRef](#)]
9. Zhao, M.; Akansu, A.N. UEP of progressive images in wireless channels. In Proceedings of the Vehicular Technology Conference Fall 2000, Boston, MA, USA, 24–28 September 2000.
10. Zhao, M.; Akansu, A.N. Optimization of dynamic UEP schemes for embedded image sources in noisy channels. In Proceedings of the International Conference on Image Processing (ICIP), Vancouver, BC, Canada, 10–13 September 2000.
11. Yang, X.; Yuan, D.; Ma, P.; Jiang, M. New research on unequal error protection (UEP) property of irregular LDPC codes. In Proceedings of the First IEEE Consumer Communications and Networking Conference (CCNC), Las Vegas, NV, USA, 5–8 January 2004.
12. Ma, P.; Kwak, K.S. Modulation-assisted UEP-LDPC codes in image transmission. In Proceedings of the 9th International Symposium on Communications and Information Technology (ISCIT), Icheon, Korea, 28–30 September 2009.
13. Liao, Y.; Qiu, M.; Yuan, J. Design and Analysis of Delayed Bit-Interleaved Coded Modulation with LDPC Codes. *IEEE Trans. Commun.* **2021**, *69*, 3556–3571. [[CrossRef](#)]
14. Xu, B.; Zhang, Z.M.; Zhang, E.Y.; He, Y.L. Research on Unequal Error Protection with Irregular LDPC and Application on Image Transmission. In Proceedings of the 2nd International Congress on Image and Signal Processing (ICISP), Tianjin, China, 17–19 October 2009.
15. Zhang, W.; Jing, X.; Zhang, Z.; Chen, Q. Image transmission with UEP-LT over MIMO channels. In Proceedings of the 22nd Wireless and Optical Communication Conference (WOCC), Chongqing, China, 16–18 May 2013.
16. Ninkovic, V.; Vukobratovic, D.; Häger, C.; Wymeersch, H.; Graell i Amat, A. Autoencoder-Based Unequal Error Protection Code. *IEEE Commun. Lett.* **2021**, *25*, 3575–3579. [[CrossRef](#)]
17. Yao, X.; Wan, H.; Ma, X. A type-aware coding approach for unequal message protection. *Phys. Commun.* **2022**, *53*, 101721. [[CrossRef](#)]
18. Chung, S.-Y.; Forney, G.D.; Richardson, T.J.; Urbanke, R. On the Design of Low-density Parity-check Codes within 0.0045 dB of the Shannon Limit. *IEEE Commun. Lett.* **2001**, *5*, 58–60. [[CrossRef](#)]
19. Fossorier, M.P.C. Iterative reliability-based decoding of low-density parity check codes. *IEEE J. Sel. Areas Commun.* **2001**, *5*, 908–917. [[CrossRef](#)]
20. Dai, L.; Fang, Y.; Yang, Z.; Chen, P.; Li, Y. Protograph LDPC-Coded BICM-ID With Irregular CSK Mapping in Visible Light Communication Systems. *IEEE Trans. Veh. Technol.* **2021**, *70*, 11033–11038. [[CrossRef](#)]
21. Chen, P.; Wang, L.; Lau, F.C.M. One Analog STBC-DCSK Transmission Scheme not Requiring Channel State Information. *IEEE Trans. Circuits Syst. I Regul. Pap.* **2013**, *60*, 1027–1037. [[CrossRef](#)]
22. Chen, P.; Cai, K.; Zheng, S. Rate-Adaptive Protograph LDPC Codes for Multi-Level-Cell NAND Flash Memory. *IEEE Commun. Lett.* **2018**, *22*, 1112–1115. [[CrossRef](#)]
23. Chen, L.; Chen, P.; Lin, Z. Artificial Intelligence in Education: A Review. *IEEE Access* **2020**, *8*, 75264–75278. [[CrossRef](#)]
24. Chen, C.; Xiang, J.; Ye, Z.; Yan, W.; Wang, S.; Wang, Z.; Chen, P.; Xiao, M. Deep Learning-Based Energy Optimization for Edge Device in UAV-Aided Communications. *Drones* **2022**, *6*, 139. [[CrossRef](#)]
25. Fang, Y.; Bu, Y.; Chen, P.; Lau, F.C.M.; Otaibi, S.A. Irregular-Mapped Protograph LDPC-Coded Modulation: A Bandwidth-Efficient Solution for 6G-Enabled Mobile Networks. *IEEE Trans. Intell. Transp. Syst.* **2021**, early access. [[CrossRef](#)]
26. Razaghi, P.; Yu, W. Bilayer Low-density Parity-check Codes for Decode-and-Forward in Relay Channels. *IEEE Trans. Inf. Theory* **2007**, *53*, 3723–3739. [[CrossRef](#)]
27. Vahabzadeh, O.; Salehi, M. Design of bilayer lengthened LDPC codes for Rayleigh fading relay channels. In Proceedings of the 45th Annual Conference on Information Sciences and Systems, Baltimore, MD, USA, 23–25 March 2011.
28. Van Nguyen, T.; Nosratinia, A.; Divsalar, D. Bilayer protograph codes for half-duplex relay channels. *IEEE Trans. Wirel. Commun.* **2013**, *12*, 1969–1977. [[CrossRef](#)]
29. Fang, Y.; Bi, G.; Guan, Y.L.; Lau, F.C. A survey on protograph LDPC codes and their applications. *IEEE Commun. Surv. Tutor.* **2015**, *17*, 1989–2016. [[CrossRef](#)]

30. Dai, J.; Tan, K.; Si, Z.; Niu, K.; Chen, M.; Poor, H.V.; Cui, S. Learning to decode protograph LDPC codes. *IEEE J. Sel. Areas Commun.* **2021**, *39*, 1983–1999. [[CrossRef](#)]
31. Cover, T.; Gamal, A.E. Capacity theorems for the relay channel. *IEEE Trans. Inf. Theory* **1979**, *25*, 572–584. [[CrossRef](#)]
32. Lengwehasatit, K.; Ortega, A. Scalable Variable Complexity Approximate forward DCT. *IEEE Trans. Circuits Syst. Video Technol.* **2004**, *14*, 1236–1248. [[CrossRef](#)]
33. Triantafyllidis, G.A.; Tzovaras, D.; Strintzis, M.G. Blocking Artifact Detection and Reduction in Compressed Data. *IEEE Trans. Circuits Syst. Video Technol.* **2002**, *12*, 877–890. [[CrossRef](#)]
34. Banerjee, S.; Choudhary, A.; Pal, S. Empirical Evaluation of K-Means, Bisecting K-Means, Fuzzy C-Means and Genetic K-Means Clustering Algorithms. In Proceedings of the IEEE International WIE Conference on Electrical and Computer Engineering (WIECON-ECE), Pune, India, 19–21 December 2016.
35. Singh, U.P.; Chouhan, S.S.; Jain, S. Images as Graphical Password: Verification and analysis using non-regular low-density parity check coding. *Int. J. Inf. Technol.* **2020**, *1*, 41. [[CrossRef](#)]
36. Chouhan, S.S.; Koul, A.; Singh, U.P. Image Segmentation Using Computational Intelligence Techniques: Review. *Arch. Comput. Methods Eng.* **2018**, *64*, 533–596. [[CrossRef](#)]
37. Chouhan, S.S.; Koul, A.; Singh, U.P. Soft computing approaches for image segmentation: A survey. *Multimed. Tools Appl.* **2018**, *77*, 28483–28537. [[CrossRef](#)]
38. Chouhan, S.S.; Koul, A.; Singh, U.P. Image segmentation using fuzzy competitive learning based counter propagation network. *Multimed. Tools Appl.* **2019**, *5*, 35263–35287. [[CrossRef](#)]